Density Functional Theory Study on OH-Initiated Atmospheric Oxidation of *m*-Xylene

Jiwen Fan[†] and Renyi Zhang*

Department of Atmospheric Sciences and Department of Chemistry, Texas A&M University, College Station, Texas 77843

Received: September 23, 2007; In Final Form: February 18, 2008

The OH-initiated oxidation reactions of *m*-xylene are investigated using density functional theory. The structures, energetics, and relative stability of the OH-*m*-xylene reaction intermediate radicals have been determined, and their activation barriers have been analyzed to assess the energetically favorable pathways to propagate the oxidation. OH addition occurs preferentially at the two ortho positions with the branching ratios of 0.97, 0.02, and 0.01 for ortho, meta, and ipso additions, respectively. The results reveal that the OH-*m*-xylene-O_2 peroxy radicals preferentially cyclize to form bicyclic radicals under atmospheric conditions rather than reacting with NO to lead to ozone formation, and the decomposition to O_2 and the hydroxyl *m*-xylene adduct is competitive with the cyclization process. The bicyclic radicals of *m*-xylene formed from the major OH-addition pathways (i.e., ortho positions) are more probable to form bicyclic peroxy radicals by reacting with O_2. This study provides thermochemical and kinetic data of the OH-initiated reactions of *m*-xylene for assessment of the role of aromatic hydrocarbons in photochemical production of ozone, toxic products, and secondary organic aerosols.

1. Introduction

Aromatic hydrocarbons such as benzene, toluene, and xylenes are important constituents of gasoline, vehicle emissions, and ambient air in urban areas and significantly contribute to ozone, photochemical smog, and secondary organic aerosol (SOA) formation.[1−10] Recently, evidence has been suggested for the formation of potentially toxic and mutagenic epoxide products from oxidation of aromatic hydrocarbons.[6] *m*-Xylene represents a major component of aromatic hydrocarbons and is highly reactive with respect to ozone and SOA formation.

In the atmosphere, the reaction of *m*-xylene with hydroxyl radicals (OH) corresponds to the major atmospheric loss process during daylight hours. Its reaction rate with OH radicals is on the order of 10^{-11} cm^3 molecule^{-1} s^{-1},[11] much higher than that of the OH-toluene reaction.[7] The OH-initiated reaction of *m*-xylene results in minor H-abstraction from the methyl group to form methylbenzyl radicals (about 4%) and major OH addition to the aromatic ring to form *m*-xylene-OH adducts (about 96%).[12−14] The OH-*m*-xylene adducts are expected to react with O_2, forming primary peroxy radicals under atmospheric conditions.[15−16] The fate of the xylene peroxy radicals is governed by competition between reaction with NO to form alkoxy radicals and cyclization to form bicyclic radicals. On the basis of theoretical studies of toluene and *p*-xylene,[7,8] the cyclization reaction is expected to be more important than reaction with NO under typical atmospheric conditions. The detection of large yields of methylglyoxal, 4-oxo-2-pentenal and glyoxal in laboratory studies supports the preference of cyclization reaction to form bicyclic radicals.[4,17] The bicyclic radicals can form epoxide radicals by unimolecular rearrangement or form (secondary) bicyclic peroxy radicals by reacting with O_2.[17] Scheme 1 illustrates the likely pathways of *m*-xylene oxidation initiated by OH, showing that the oxidation occurs in multiple steps and isomeric pathways. For example, OH addition to *m*-xylene initially results in four distinct structural *m*-xylene-OH adduct isomers; subsequent reactions of the *m*-xylene-OH adducts with O_2 and cyclization of the peroxy radicals incur additional isomeric branching.

The rate constant of the initial *m*-xylene-OH reaction has been investigated at different temperatures and pressures by experimental studies.[11,14,18−23] The recommended room-temperature rate constant for *m*-xylene is 23.6×10^{-12} cm^3 molecule^{-1} s^{-1} with the uncertainty of ±25%.[23] Some products from OH-initiated *m*-xylene oxidation have been identified and quantified by experimental work.[4,6,17,19,24−28] Three products, methylglyoxal, 4-oxo-2-pentenal, and 2-methyl-4-oxo-2-butenal, and dimethylphenols exhibited a dependence of the formation yields on O_2 and NO concentrations.[4,14] Smith et al. reported significant yields of methyglyoxal and 4-oxo-2-pentenal (about 40 and 12%, respectively), indicating that the ring-cleavage pathway involving the bicyclic peroxy radical represents the major pathway for the oxidation of *m*-xylene initiated by OH.[4] The most recent laboratory study by Zhao et al. quantified three ring-opening products, that is, 2-methyl-4-oxo-2-penetal (4.9 ± 0.52)%, diunsaturated dicarbonyls (7.8 ± 1.0)%, and epoxy carbonyls (2.2 ± 0.20)%.[17]

Currently, the explicit mechanism of *m*-xylene oxidation following the initial OH attack remains highly uncertain. In previous experimental product studies of m-xylene, less than 50% of the reacted carbon has been typically identified in the product distributions.[4,17,24−25] The difficulty in accounting for the remaining fraction of reacted carbon largely lies in the fact that the many organic intermediates involved in the *m*-xylene-OH oxidation have not been unambiguously identified. In contrast, theoretical studies are useful in assessing the preferred reaction pathways of aromatic intermediate radicals and, consequently, evaluating the mechanisms of the aromatic oxidation.[7,8] In a previous study by Andino et al., some of the

* Corresponding author: E-mail: zhang@ariel.met.tamu.edu.
[†] Current Address: Climate Physics, Pacific Northwest National Laboratory, PO Box 999, MSIN k9-24, Richland, WA 99352.

10.1021/jp077648j CCC: $40.75
Published on Web 03/27/2008

SCHEME 1: Mechanistic Diagram of the *m*-Xylene-OH Reaction System

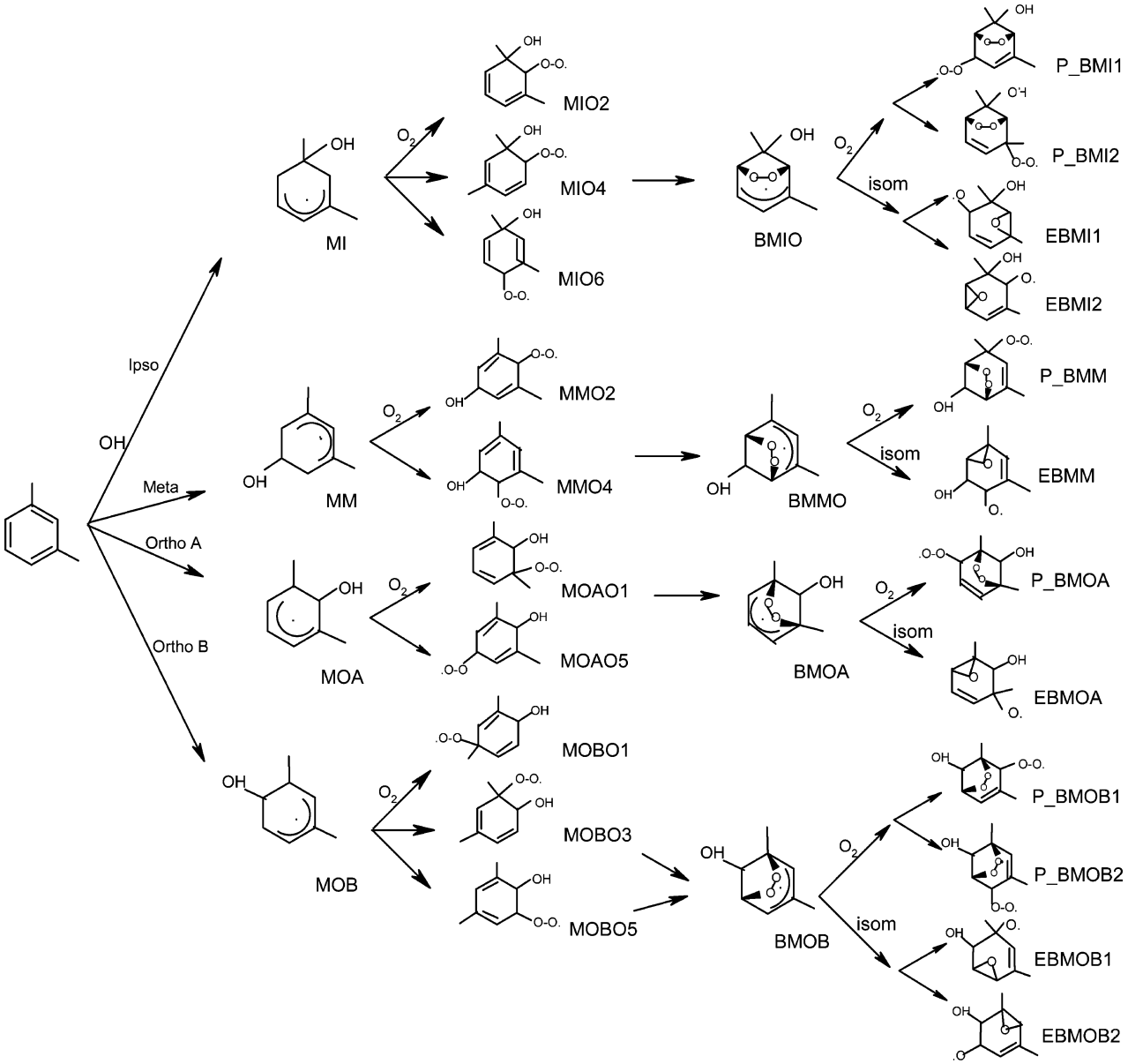

intermediate species of the OH-*m*-xylene reactions have been theoretically investigated.[16] In this work, we present a theoretical investigation of the oxidation reactions from the addition of OH to *m*-xylene, including the formation of aromatic peroxy, bicyclic, epoxide, and bicyclic peroxy radicals. The rate constants and isomeric branching of OH-*m*-xylene reactions are calculated. Reaction energies for the formation of the aromatic radicals are obtained to determine their relative stability and reversibility, and the energetically favorable pathways are determined to propagate the *m*-xylene oxidation through the assessment of the activation barriers.

2. Theoretical Method

We performed the theoretical calculations on an SGI Origin 3800 supercomputer using the GAUSSIAN 98 software package,[29] similar to those in our previous studies for OH-initiated oxidation of toluene and *p*-xylene.[7,8] All radicals were treated with the unrestricted density functional theory (UDFT) formulation. Geometry optimization was executed using Becke's three-parameter hybrid exchange functional employing the LYP correction function (B3LYP) in conjunction with the split valence polarized basis set 6-31G(d,p).

Previous theoretical studies have been carried out to evaluate the quantum chemical methods applicable to the aromatic oxidation reactions (see, for example, ref 30 and references therein).[7−9,16,30] For the initial OH addition to toluene, the results revealed that the DFT method predicted binding energies and activation energies in good agreement with the experimental values, compared to ab initio multiconfigurational calculations (CASSCF) for geometry optimization and second-order MP2 and coupled-cluster theory (CCSD(T)) for single-point energy calculations.[7−9] The correlated methods employing MP2 and CCSD(T) produced significantly higher activation energies than the experimental value because of contamination of unrestricted Hartree−Fock wave function from higher spin states in the single-point energy calculations of the transition states. The CASSCF and CSSPT2 methods also produced higher activation energies than the experimental values.

The transition state (TS) was searched by using the TS keyword in geometry optimization at the B3LYP/6-31G(d,p) level of theory. Once an initial geometry optimization reached convergence, a frequency calculation was performed to determine whether this optimized geometry represented a first-order saddle point. A transition state was identified by finding only

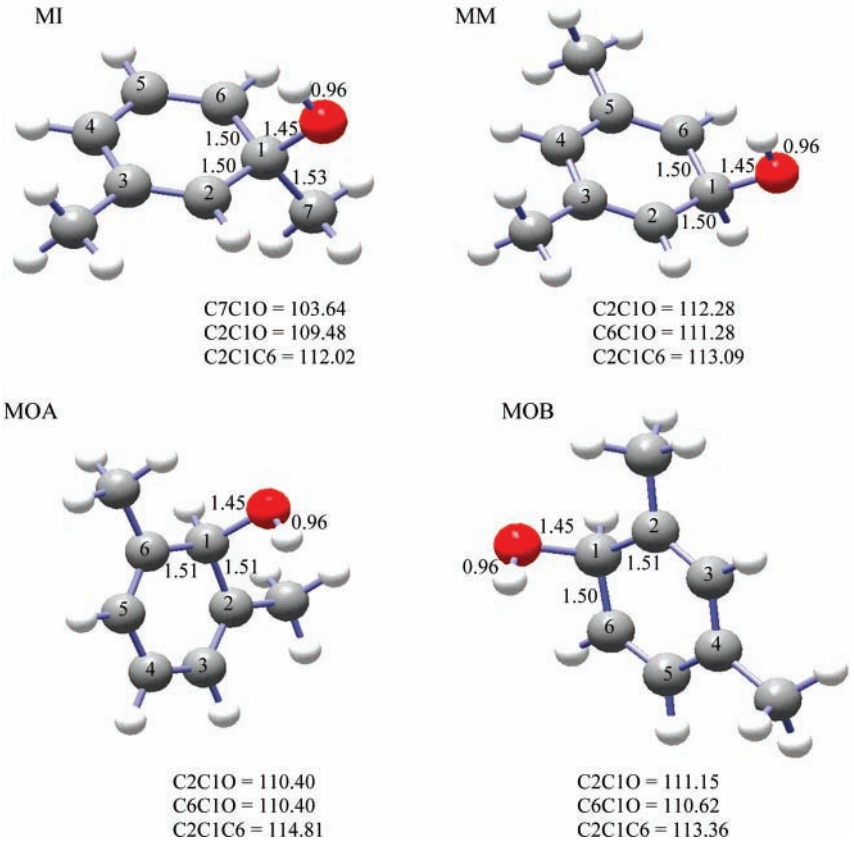

Figure 1. Optimized geometries of *m*-xylene-OH adducts at the B3LYP/6-31G(d,p) level of theory.

one imaginary component in the calculated vibrational frequencies. The vibrational modes along the reaction coordinates were examined to verify that these modes represented the trend along the intended reaction coordinate. We performed additional calculations using the intrinsic reaction coordinate (IRC) method,[30,31] confirming that each TS uniquely connected the reactant to the product.

Rate constants of the unimolecular (k_{uni}) and bimolecular (k_b) reactions of the aromatic intermediate radicals were calculated using classic transition state theory (TST). The high-pressure limit unimolecular rate constant is expressed by[31−33]

$$k_{uni} = \frac{k_b T}{h} \frac{Q^{\ddagger}_{AB}}{Q_{AB}} \exp\left(-\frac{E_a}{kT}\right) \quad (1)$$

where k_b is the Boltzmann constant, h is the Plank's constant, T is the temperature, $Q_{AB}^{\ddagger}$ is the partition function for all degrees of freedom of the transition state with the vibrational frequency corresponding to the reaction coordinate removed, Q_{AB} is the complete partition function of the reactant, and E_a is the zero-point corrected activation energy. The association rate is related to the dissociation rate by the equilibrium constant (K_{eq})[31−33]

$$\frac{k_{rec}}{k_{uni}} = K_{eq} = \frac{Q_{AB}}{Q_A Q_B} \exp\left(\frac{RE}{kT}\right) \quad (2)$$

where Q_{AB} is the partition function of the dissociating species, Q_A and Q_B are the partition functions of the fragmentation products, and RE is the zero-point corrected reaction or binding energy. The partition functions were evaluated by treating the rotational and translational motion classically and treating vibrational modes quantum-mechanically. Unscaled vibrational frequencies and moments of inertia were calculated at the B3LYP/6-31G(d,p) level, and the reaction and activation energies were taken at the zero-point corrected B3LYP/6-31G(d,p) level. No tunneling or other curve cutting approximations were made in the TST rate calculations

3. Results and Discussion

3.1. *m*-Xylene-OH Adducts. Four possible isomers of OH-*m*-xylene adducts, that is, ipso, meta, and two ortho isomers are formed from OH addition to *m*-xylene (Scheme 1), with two ortho isomers of MOA and MOB. Figures 1 and 2 depict the optimized geometries of the four adducts and their corresponding transition states (TS) obtained at the B3LYP/6-31G(d,p) level of theory. Addition of OH to *m*-xylene leads to a lengthening of C−C bonds adjunct to the site of addition. For the ipso isomer (MI), the C−C bond lengths are increased by 0.10 Å between C1−C2 and C1−C6 and by 0.02 Å between C1 and C7 (the methyl carbon). The increased C−C bond length adjacent to the OH addition site reflects an increased character, as electron density is transferred to the newly formed C−O bonds. Similar C−C bonding characteristics are observed for the other isomers, that is, MM, MOA, and MOB: the bond lengths are increased by 0.10−0.11 Å between C1−C2 and C1−C6. The C−O bond distance is 1.45 Å for all isomers. In the transition states, the C−O distances are 2.05, 2.03, 2.11, and 2.07 Å for MI, MM, MOA, and MOB, respectively. A comparison of the structures of *m*-xylene, the adduct isomers, and the transition states clearly reveals the intermediate features in the transition state structures. The calculated spin eigenvalues, $<S^2>$, are 0.788, 0.787, 0.787, and 0.785 for MI, MM, MOA, and MOB, respectively. After the $S + 1$ component is annihilated, the values of $<S^2>$ are reduced to 0.751 for all isomers, nearly identical to the exact value of a pure doublet. This implies that contamination of the unrestricted Hartree−Fock wave function from higher spin states is negligible.

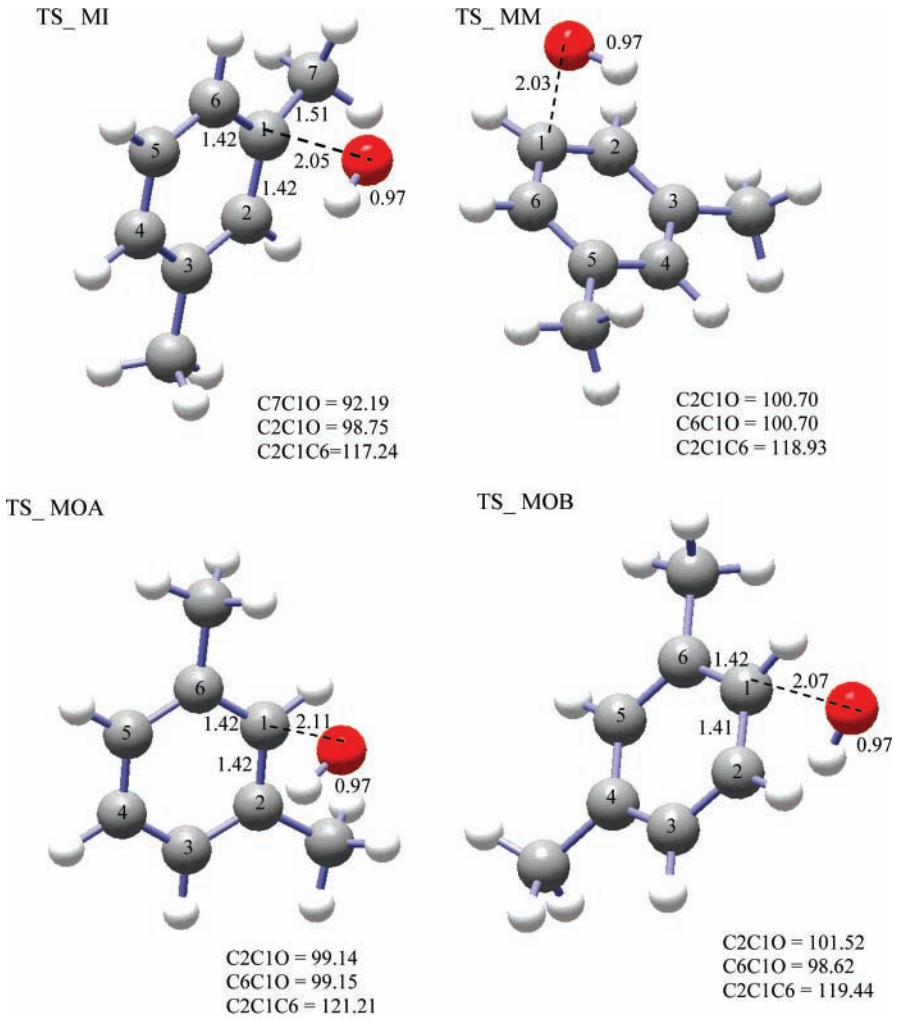

Figure 2. Transition states of *m*-xylene-OH adducts at the B3LYP/6-31G(d,p) level of theory.

TABLE 1: Zero-Point Corrected Reaction Energies (RE), Activation Energies (E_a), High-Pressure Rate Constants (k_{rec} and k_{uni}) at 300 K, Equilibrium Constants (K), and Branching Ratios (R) of the *m*-Xylene-OH Reactions

species[a]	RE kcal mol^{-1}	E_a kcal mol−1	k_{rec} cm^{3}mole^{-1}s $^{-1}$	k_{uni} s $^{-1}$	K	R	k (tot) cm^{3}mole^{-1}s $^{-1}$
MI	−16.39	−1.72	3.62×10^{-13}	6.35×10^{2}	1.40×10^{4}	0.01	
MM	−16.18	−1.62	1.06×10^{-12}	1.09×10^{3}	2.41×10^{4}	0.02	
MOA	−18.77	−4.80	3.52×10^{-11}	1.00×10^{3}	8.64×10^{5}	0.60	
MOB	−18.26	−3.84	2.23×10^{-11}	4.46×10^{2}	1.23×10^{6}	0.37	5.85×10^{-11}

[a] The species labeled corresponds to the reaction pathway leading to its formation, as shown in Scheme 1.

The calculated zero-point corrected reaction (binding) energies (RE) and activation energies (E_a) for OH-*m*-xylene adduct formation are provided in Table 1 at the B3LYP/6-31G(d,p) level. The reaction energies for MI and MM are nearly identical, with the values of −16.4 and −16.2 kcal mol^{-1}, respectively. The two ortho isomers MOA and MOB are about 2 kcal mol^{-1} more stable than those for MI and MM. The activation energies for the formation of MOA and MOB are lower than those for MI and MM by about 2 kcal mol^{-1}. For all OH addition pathways, the predicted activation energies are negative at the B3LYP/6-31G(d,p) level. Also, there appears to be a correlation between the reaction and activation energies for initial addition of OH to *m*-xylene. On the basis of the calculated activation energies and the transition state theory (TST), the high-pressure rate constants for the formation of the OH-*m*-xylene adduct radicals (k_{rec}) are calculated. As shown in Table 1, the calculated high-pressure rate constants for MI, MM, MOA, and MOB are 3.6×10^{-13}, 1.1×10^{-12}, 3.5×10^{-11}, and 2.2×10^{-11} cm^3 molecule^{-1} s^{-1}, respectively. The formation rates of MOA and MOB are faster than those of MI and MM, because MOA and MOB are more stable and the activation energies for their formation are lower. The predicted overall rate constant for OH addition to *m*-xylene is 5.9×10^{-11} cm^3 molecule^{-1} s^{-1}. This value is higher than the recommended value of 2.4×10^{-11} cm^3 molecule^{-1} s^{-1} [23] but is explainable considering the combined uncertainties of theoretical and experimental studies. Because the OH-*m*-xylene reaction results in minor H-abstraction from one methyl group to form a methylbenzyl radical (about 4%),[23] we did not consider the H-abstraction pathway in the present work. Nevertheless, the H-atom abstraction process can be computed to assess the quantitative and qualitative success of the quantum chemical methods for aromatic systems in future studies.

The decomposition rate constants for OH-*m*-xylene adduct isomers are also calculated with the values of 6.4×10^{2}, 1.1×10^{3}, 1.0×10^{3}, and 4.5×10^{2} s^{-1} for MI, MM, MOA, and

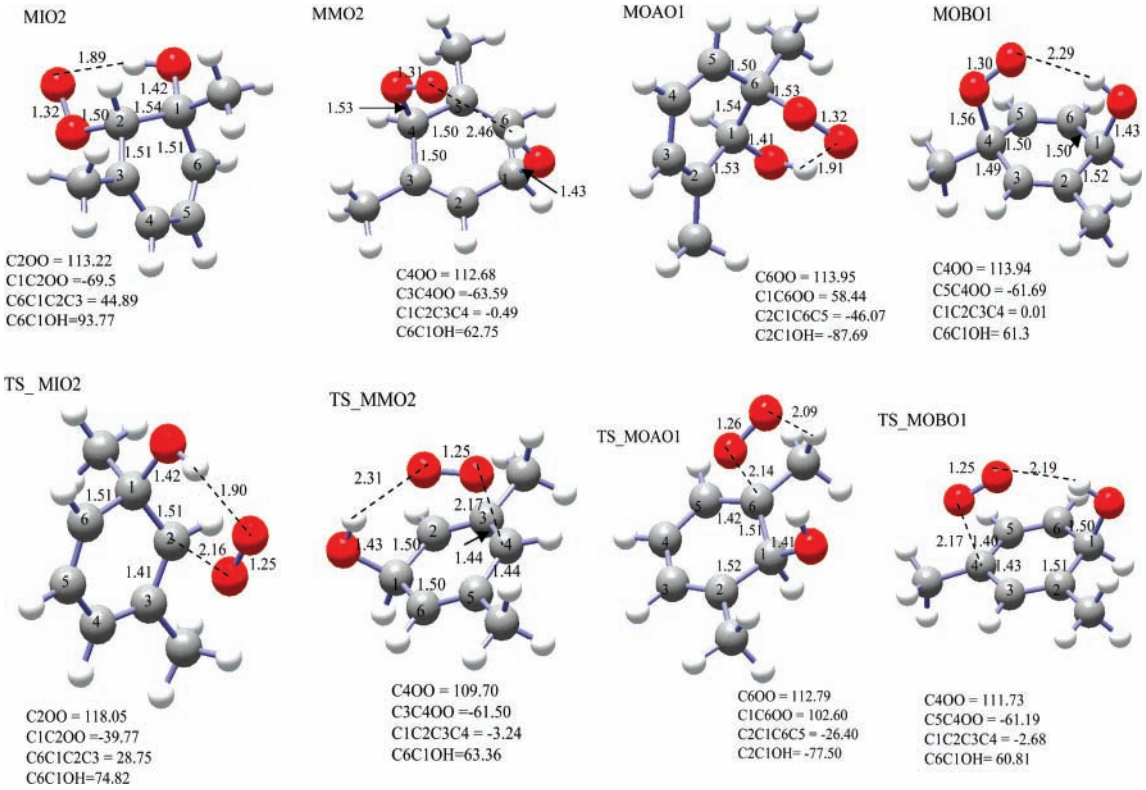

Figure 3. Optimized geometries of the representative primary peroxy radicals and their corresponding transition states at the B3LYP/6-31G(d,p) level of theory.

MOB, respectively (Table 1). The branching ratio for each OH addition pathway (*R*) is determined on the basis of the calculated high-pressure rate constants (Table 1). For the formation of MI, MM, MOA, and MOB, the branching ratios are predicted as 0.01, 0.02, 0.60, and 0.37, respectively, suggesting a strong preference for the two ortho additions of OH to *m*-xylene. The previous theoretical study by Andino et al.[16] also suggested a dominant ortho OH addition to *m*-xylene because of their larger stability.

3.2. OH-*m*-Xylene-O_2 Peroxy Radicals. Under atmospheric conditions, the OH-*m*-xylene adducts are expected to react with O_2 to form the primary peroxy radicals. Addition to the ipso OH-*m*-xylene adduct forms three possible structural isomers of peroxy radicals, MIO2, MIO4, and MIO6 (Scheme 1). O_2 addition to the meta adduct results in two plausible peroxy radical isomers, that is, MMO2 and MMO4. Two possible peroxy radical isomers are formed from O_2 addition to MOA and three are produced from O_2 addition to MOB, corresponding to MOAO1, MOAO5, MOBO1, MOBO3, and MOBO5. Figure 3 shows the optimized geometries of the lowest-energy conformations of MIO2, MMO2, MOAO1, and MOBO1 and their corresponding transition states at the B3LYP/6-31G(d,p) level. For the peroxy radicals, the energetically favorable conformation corresponds to O_2 addition on the same side of the benzene ring as the hydroxyl group, resulting in a stabilization of about 5−8 kcal mol^{-1}. The C−C bond lengths adjacent to the site of O_2 addition are increased, as electron density in the bond is transferred to the newly formed C−O bonds. There exists intramolecular hydrogen bond in the peroxy radicals. The hydrogen bonding involves interaction between the terminal oxygen of the peroxy group and the hydrogen of the OH group, forming a six-membered ring. The distance of intramolecular hydrogen bond ranges from 1.89 to 2.46 Å with the latter value corresponding to rather weak hydrogen bond. Note that the B3LYP/6-31G(d,p) method may suffer from basis set superposition error (BSSE) and that hydrogen bonding may be overestimated by basis sets without diffuse functions.[34] The BSSE effect on the calculations of the energetics of aromatic peroxy radicals needs to be evaluated in future theoretical studies. Compared with the geometries of the OH-*m*-xylene adducts shown in Figure 1, the addition of O_2 to the OH-*m*-xylene adducts results in a shortening of the C−O(H) bond. For example, the shortening of the C−O(H) bonds for MIO2, and MOAO1 is about 0.04 Å, while it is only about 0.02 for MMO2 and MOBO1 (Figure 3).

In the transition states (TS), the newly formed C−O bond lengths for the representative peroxy radicals range from 2.14 to 2.17 Å. As shown in Figure 3, the intramolecular hydrogen bond also exists in the TS structures. The hydrogen bond lengths are between 1.90 and 2.31 Å. Note that the hydrogen bond in the TS_MOAO1 goes to the neighboring methyl group due to the interaction of the lone pairs between the oxygen atom in the peroxy group and the hydrogen atom in the methyl group. The oxygen bond rotates to shorten the distance between O and H in the methyl group. On the other hand, the distance between O atom in the peroxy group and the H atom in the hydroxyl group is 2.4 Å. The transition state of MOBO5 exhibits the similar intramolecular hydrogen bond as TS_MOAO1.

Table 2 shows the zero-point corrected reaction energies for the formation of the peroxy radicals. The binding energies of the peroxy radicals range from 4.5 to 7.0 kcal mol^{-1}. O_2 addition at C2 (MIO2) and C4 (MMO4) of the aromatic ring represents the most stable isomers for the ipso and meta OH-*m*-xylene adduct. For the two ortho OH-*m*-xylene adducts (MOA and MOB), MOAO1 and MOBO5 represent the most stable peroxy isomers, respectively. Hydrogen-bonding plays a role in stabilizing the peroxy radicals. For example, the MIO2 has the strongest hydrogen bonding among the peroxy radicals formed from ipso OH-*m*-xylene adduct, with a hydrogen bond length of 1.89 Å.

TABLE 2: Zero-Point Corrected Reaction Energies (RE) and Activation Energies (E_a) for the *m*-Xylene-OH−O_2 Reactions

type	reaction	RE	E_a	type	reaction	RE	E_a
ipso	MI + O_2 → MIO2	−5.44	4.23	ortho A	MOA + O_2 → MOAO1	−5.17	2.6
	MI + O_2 → MIO4	−4.83	−1.3		MOA + O_2 → MOAO5	−4.78	−0.68
	MI + O_2 → MIO6	−5.16	1.62		MOAO1 → BMOA	−7.02	9.11
	MIO4 → BMIO	−8.89	10.42		BMOA → EBMOA	−15.63	9.27
	BMIO → EBMI1	−16.85	5.61		BMOA + O_2 → P_BMOA	−13.02	0.83
	BMIO → EBMI2	−15.13	5.61				
	BMIO + O_2 → P_BMI1	−13.44	15.23				
meta	MM + O_2 → MMO2	−5.75	2.61	ortho B	MOB + O_2 → MOBO1	−4.53	−1.2
	MM + O_2 → MMO4	−6.98	−2.08		MOB + O_2 → MOBO3	−5.13	2.58
	MMO4 → BMMO	−8.54	9.71		MOB + O_2 → MOBO5	−6.57	3.56
	BMMO → EBMM	−16.32	4.23		MOBO3 → BMOB (a)	−6.80	9.32
					MOBO5 → BMOB (b)	−5.37	10.76
					BMOB → EBMOB2	−17.68	10.17
					BMOB + O_2 → P_BMOB1	−14.16	−0.17
					BMOB + O_2 → P_BMOB2	−14.44	0.16

The activation energies to form the peroxy radicals are also included in Table 2. The activation barriers are typically less than 5 kcal mol^{-1} with the largest activation barrier of about 4.2 kcal mol^{-1} for MIO2. The activation energies for the formation of MIO4, MMO4, MOAO5, and MOBO1 are slightly negative. For the B3LYP/6-31G(d,p) method, the $<S^2>$ values in calculating the TS energies for the primary peroxy radicals are about 1.10−1.20 and 0.76−0.77 before and after annihilation, respectively. Note that although the peroxy radicals MIO2, MOAO1, and MOBO5 represent the most stable structures for O_2 addition to the different *m*-xylene-OH adducts, their activation barriers are slightly higher than those of the other isomers formed from the same OH-*m*-xylene adducts. Hence, in contrast to the OH-*m*-xylene adducts there is a lack of correction between the reaction and activation energies for the peroxy radicals. Andino et al.[16] employed UHF/PM3 methods for geometry optimizations and a single-point calculation at the B3LYP/6-31G(d,p) level of theory and calculated the activation barriers of 6.5 and 10.0 kcal mol^{-1} for the formation of the peroxy radicals from MOA and MOB, respectively. Those values are somewhat higher than our calculations.

The high-pressure limit rate constants of O_2 addition to the OH-*m*-xylene adducts at B3LYP/6-31G(d,p) level are calculated and presented in Table 3. The calculated rate constants range from 10^{-17} to 10^{-13} cm^3 $molecule^{-1}$ s^{-1}, showing a large difference in the rate constants for the isomers of the peroxy radicals. For the ipso OH-*m*-xylene adduct, O_2 addition occurs with the rate constants of 2.0×10^{-17}, 1.6×10^{-13}, and 1.0×10^{-15} cm^3 $molecule^{-1}$ s^{-1} for MIO2, MIO4, and MIO6, respectively. The decomposition rates of those peroxy radicals are high (up to 10^{10} s^{-1}), indicating that the O_2 addition to the OH−*m*-xylene adducts corresponds to a reversible process. Because of the relatively small binding energies of the peroxy radicals, the OH-*m*-xylene adducts reaction with O_2 proceeds reversibly, and the equilibrium favors peroxy radical decomposition (the equilibrium constants (K) for the reactions of formation of the peroxy radicals are small). The close relative stability and reversibility of the peroxy radicals suggest that all isomers of the peroxy radicals are likely to form. The relative stability and activation barriers of the peroxy radicals, however, have little effect on isomeric branching, because propagation of the *m*-xylene oxidation is largely determined by the exit channel of the peroxy radicals. The steady-state concentrations of the peroxy radicals are determined by recombination of the adduct with O_2, dissociation of the peroxy radicals, and the exit channel of the peroxy radicals, that is, reaction with NO to form alkoxy radicals, rearrangement to form bridged bicyclic radicals, or H-abstraction to form phenols.

3.3. Bicyclic Radicals. The OH-*m*-xylene-O_2 peroxy radicals may cyclize to form bridged bicyclic radicals. For ipso and meta OH addition, the peroxy radicals MIO4 and MMO4 cyclize to form BMIO and BMMO, respectively. The bicyclic radical BMOA is formed from the ortho A OH addition, and the peroxy radicals MOBO3 and MOBO5 from the ortho B OH addition undergo cyclization to form an identical bicyclic radical BMOB. BMIO, BMMO, BMOA, and BMOB are the only stable bicyclic radicals, while the other bicyclic radicals possess structures that are about 20 kcal mol^{-1} higher in energy. The large stability of

TABLE 3: Calculated High-Pressure Limit Rate Constants of Intermediate Radicals for the *m*-Xylene-OH−O_2 Reactions at 300 K[a]

species[b]	k	k^{-1}	K	species	k	k^{-1}	K
MIO2	2.02×10^{-17}	2.41×10^{6}	2.06×10^{-4}	MOAO1	3.09×10^{-16}	7.41×10^{7}	1.03×10^{-4}
MIO4	1.60×10^{-13}	4.62×10^{10}	8.51×10^{-5}	MOAO5	5.76×10^{-14}	1.75×10^{10}	8.09×10^{-5}
MIO6	1.03×10^{-15}	1.51×10^{8}	1.67×10^{-4}	BMOA	2.88×10^{5}	1.09×10^{1}	2.65×10^{4}
BMIO	3.77×10^{4}	4.64×10^{-2}	8.12×10^{5}	EBMOA	9.16×10^{5}	2.35×10^{-6}	3.90×10^{11}
EBMI1	4.46×10^{8}	2.62×10^{-4}	1.70×10^{12}	P_BMOA	7.86×10^{-15}	1.71×10^{3}	1.13×10^{2}
EBMI2	4.45×10^{8}	3.70×10^{-3}	1.20×10^{11}				
P_BMI1	5.45×10^{-25}	5.50×10^{-8}	2.44×10^{2}				
MMO2	1.59×10^{-16}	1.16×10^{7}	3.36×10^{-4}	MOBO1	4.06×10^{-14}	8.02×10^{10}	1.24×10^{-5}
MMO4	7.76×10^{-13}	8.84×10^{9}	2.16×10^{-3}	MOBO3	9.41×10^{-17}	7.57×10^{7}	3.06×10^{-5}
BMMO	1.38×10^{5}	1.98×10^{-1}	6.95×10^{5}	MOBO5	2.78×10^{-17}	1.13×10^{6}	6.07×10^{-4}
EBMM	3.07×10^{9}	6.36×10^{-3}	4.82×10^{11}	BMOB (a)	2.58×10^{5}	3.68	7.02×10^{4}
				BMOB (b)	1.30×10^{4}	3.68	3.54×10^{3}
				EBMOB2	1.37×10^{5}	2.64×10^{-8}	5.19×10^{12}
				P_BMOB1	2.28×10^{-14}	1.96×10^{3}	2.86×10^{2}
				P_BMOB2	1.96×10^{-14}	8.61×10^{2}	5.61×10^{2}

[a] Unimolecular rate constants are in s^{-1}, and bimolecular rate constants are in cm^3 $molecule^{-1}$ s^{-1}. Equilibrium constants K are dimensionless. [b] The species labeled corresponds to the reaction pathway leading to its formation, as shown in Scheme 1.

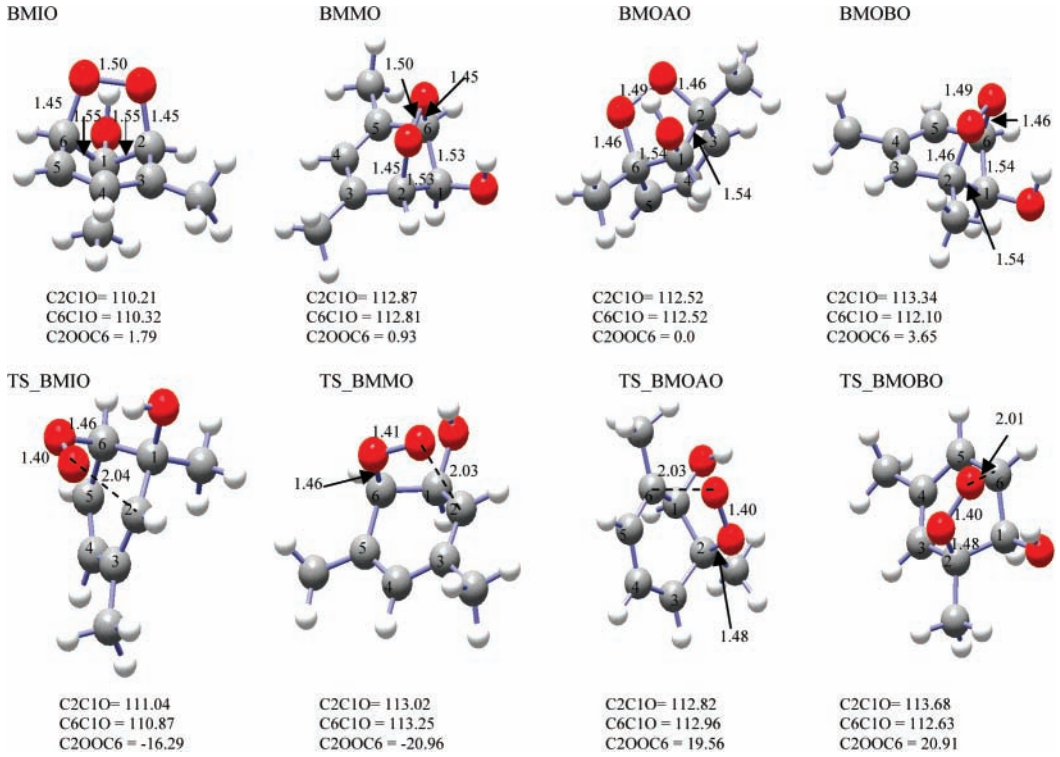

Figure 4. Optimized geometries of the bicyclic radicals and their corresponding transition states at the B3LYP/6-31G(d,p) level of theory.

BMIO, BMMO, BMOA, and BMOB is explained because these structures possess a delocalized allyl-π system, while their other structural isomers possess only one localized double bond.[7,8] In addition, formation of the non-allylically stabilized bicyclic radicals occurs via high-lying transition states, and the corresponding activation barriers are substantially higher.[7,8,30,35] Figure 4 presents the equilibrium structures and transition states of the bicyclic radicals. The two C−O bonds on the aromatic ring have a similar bond length of 1.45 or 1.46 Å for all bicyclic radicals. The distances for C−O closure at the transition states range from 2.01 to 2.04 Å. The TS structures leading to BMOB formation from MOBO3 and MOBO5 are identical, but the detailed PES around the TS regions may be very different for both pathways. The activation energies for BMOB formation from MOBO3 and MOBO5 are 9.3 and 10.8 kcal mol^{-1}, respectively (Table 2). The potential energy surface (PES) of isomerization from the peroxy to bicyclic radical for the major OH-addition pathways is illustrated in Figure 5. Isomerization of MOAO1 to BMOA is exothermic by about 7.0 kcal mol^{-1} and occurs with an activation barrier of about 9.1 kcal mol^{-1}. The exothermicities for BMOB from MOBO3 and MOBO5 are about 6.8 and 5.4 kcal mol^{-1}, respectively. The activation energy for BMOB from MOBO3 is 9.3 kcal mol^{-1}, about 1.5 kcal mol^{-1} higher than that for BMOB from MOBO5. Spin contamination associated with calculations of the bicyclic radicals and their corresponding TSs using the B3LYP/6-31G-(d,p) method is minimal, with the values of 0.77−0.78 and 0.75 before and after spin projection, respectively. The barrier heights calculated by Andino et al.[13] for the formation of the bicyclic radicals BMOA and BMOB are about 2.6 and 4.2 kcal mol^{-1} higher than our calculations, respectively.

Table 3 also shows the unimolecular rate constants of bicyclic reactions calculated at the B3LYP/6-31G(d,p) level of theory. Unimolecular formation of the bicyclic radicals has a rate of about 10^4−10^5 s^{-1}. The reversible rate constants are small, indicating that bicyclic isomerization of the peroxy radicals is almost irreversible (Table 3). The calculated rate constants for bicyclic isomerization of peroxy radicals are much faster than the first-order rate of competing reaction of peroxy radicals with NO in the atmosphere, which is only about 2 s^{-1} assuming a rate constant on the order of 10^{-11} cm^3 molecule^{-1} s^{-1} for the NO-peroxy radical reaction and an ambient NO mixing ratio of 10 parts per billion (ppb) typical of a polluted urban atmosphere.[7−8,36] This conclusion is consistent with the literature work that suggests the aromatic peroxy radicals tend to undergo bicyclic isomerization.[7,8] Note that the activation barriers for decomposition of the peroxy radicals are nearly comparable to those for isomerization (Figure 5), indicating competing pathways for the two channels.

3.4. Epoxy Radicals and Bicyclic Peroxy Radicals. The bicyclic radicals possibly undergo isomerization to form epoxy radicals or reaction with O_2 to form bicyclic peroxy radicals. The high-lying transition states and unstable structures of the nonallylic bicyclic radicals render formation of the majority of the epoxy radicals atmospherically irrelevant.[7] For the ipso OH addition, two epoxides EBM1 and EBM2 are likely formed from isomerization of BMIO. The epoxide EBMM is formed from the meta OH addition. For the ortho A OH addition, isomerization of the bicyclic radical BMOA leads to EBMOA, and two epoxide isomers, that is, EBMOB1 and EBMOB2 are possible from the ortho B OH addition. Except for EBMOB1 from BMOB, the transition states for the formation of the epoxy radicals have been identified. The equilibrium structures of the representative epoxides, along with their corresponding transition states, are shown in Figure 6. At the transition states, the distances for breaking the O−O bond range from 2.22 to 2.26 Å, and the distances for C−O closure are in the range from 2.09 to 2.18 Å. The PES for bicyclic to epoxy radical isomerization from the ortho OH addition pathways is presented in Figure 5. The epoxides are about 15−18 kcal mol^{-1} more stable than their corresponding bicyclic precursors. As shown in Figure 5, those epoxy radicals are highly stable, but the activation energies of the reactions are relatively high (about 16−18 kcal mol^{-1}). For the ipso OH addition, the epoxide

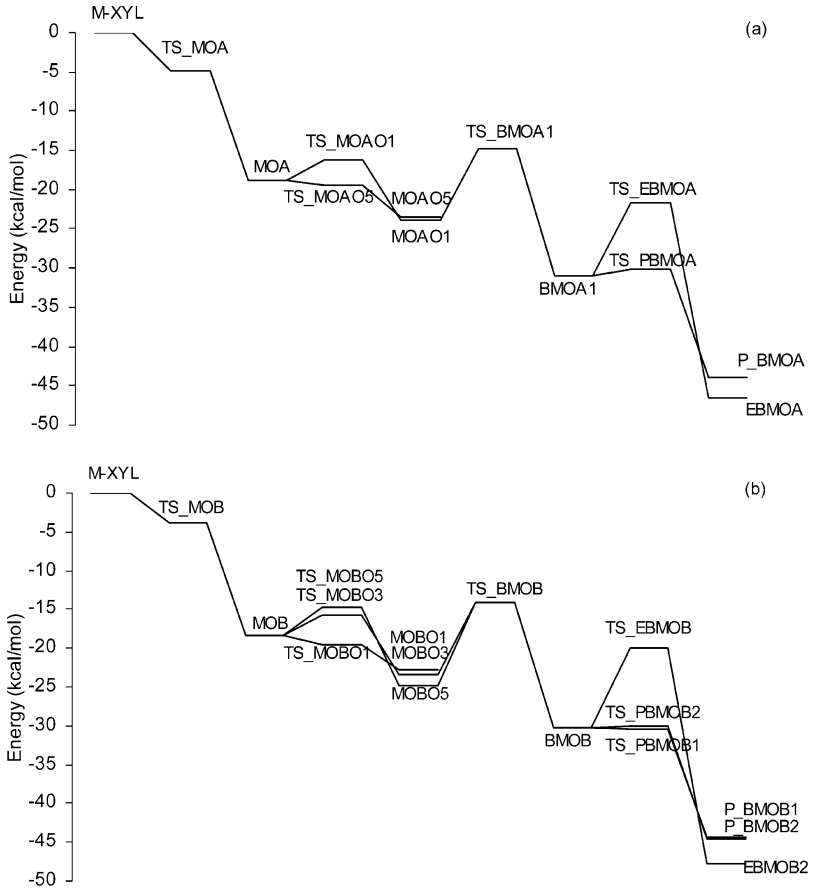

Figure 5. Potential energy surface (PES) of the major pathways for the *m*-xylene-OH reaction system: (a) for the ortho A OH addition and (b) for the ortho B OH addition.

EBM1 is more stable than EBM2, and the activation barriers to form both epoxides are comparable. Spin contamination associated with the B3LYP/6-31G(d,p) method is unimportant for the epoxy radicals, with the $<S^2>$ value close to 0.75 before projection. Spin contamination in the TS calculations of the epoxy radicals is also minimal, with the values of 0.77 and 0.75 before and after spin projection, respectively. The calculated high-pressure limit rate constants for isomerization of the thermalized bicyclic radicals to epoxides are also shown in Table 3. The unimolecular rate constants to form the epoxides EBMOA and EBMOB2 from the major OH addtion pathways are on the order of 10^5 s^{-1}. Their reversible rate constants are less than 10^{-3} s^{-1}, suggesting that the isomerization reaction of the bicyclic radicals to epoxides occurs irreversibly.

Oxygen addition to the bicyclic radicals forms bicyclic peroxy radicals. For the ipso OH addition, two bicyclic peroxy isomers P_BMI1 and P_BMI2 are possibly formed (Scheme 1). Only one bicyclic peroxy radical PBMM is possibly formed for the meta OH addition, and its transition state is also not identified. For the ortho A OH addtion, one bicyclic peroxy radical P_BMOA is formed from the addition of O_2 to the bicyclic radical BMOA. There are two possible bicyclic peroxy radicals P_BMOB1 and P_BMOB2 formed from the ortho B OH addition. The transition states are identified for the formation of the bicyclic peroxy radicals except for P_BMI2. The equilibrium structures of the representative bicyclic peroxy radicals and their corresponding transition states are shown in Figure 7. At the transition states, the distances for forming the new C−O bond are 2.20, 2.24, and 2.29 Å for P_BMI, P_BMOA, and P_BMOB2, respectively. The bicyclic peroxy radicals P_BMI1 and P_BMI2 are about 12−14 kcal mol^{-1} more stable than BMIO, but the activation barrier to form P_BMI1 is high, with the value of 15.2 kcal mol^{-1} (Table 2). The PES for the bicyclic peroxy radicals from the ortho OH addtions is showed in Figure 5. The bicyclic peroxy radicals P_BMOA, P_BMOB1 and P_BMOB2 are about 13−14 kcal mol^{-1} more stable than their bicyclic precursors, and the activation barriers for their formation are small. Also shown in Figure 5, the binding energies of the bicyclic peroxy radicals are significantly larger than those of the corresponding primary peroxy radicals at the B3LYP/6-31G(d,p) level of theory. Spin contamination for the bicyclic peroxy radicals are minimal using B3LYP/6-31G(d,p), with the values of 0.753 and 0.750 before and after annihilation, respectively. Spin contamination in the TS calculations of the bicyclic peroxy radicals is 1.20 and is 0.78 after spin projection. Through the use of semiempirical UHF/PM3 geometry optimizations combined with ab initio calculations using B3LYP/6-31G(d,p), a barrier height of 11.7 kcal mol^{-1} for the formation of the bicyclic peroxy radical of *m*-xylene was obtained by Andino et al.,[16] close to the value (15.2 kcal mol^{-1}) for formation of P_BMI1 from our calculations at the B3LYP/6-31G(d,p)//B3LYP/6-31G(d,p) level. The calculated bimolecular rate constants for the formation of P_BMI1 is small (5.5×10^{-25} cm^3 $molecule^{-1}$ s^{-1}) because of the high activation energy. The rate constants for the formation of P_BMOA, P_BMOB1 and P_BMOB2 are much larger, with the values of about 10^{-15} -10^{-14} cm^3 $molecule^{-1}$ s^{-1} (Table 3), indicating that fast formation of bicyclic peroxy radicals from the ortho OH additions.

The fate of the bicyclic radicals is determined by the competition between isomerization to epoxides and O_2 addition to form bicyclic peroxy radicals. For the ipso OH addition pathway, the effective first-order rate constant for formation of bicyclic peroxy radical P_BMI1 is about 10^{-6} s^{-1}, considerably

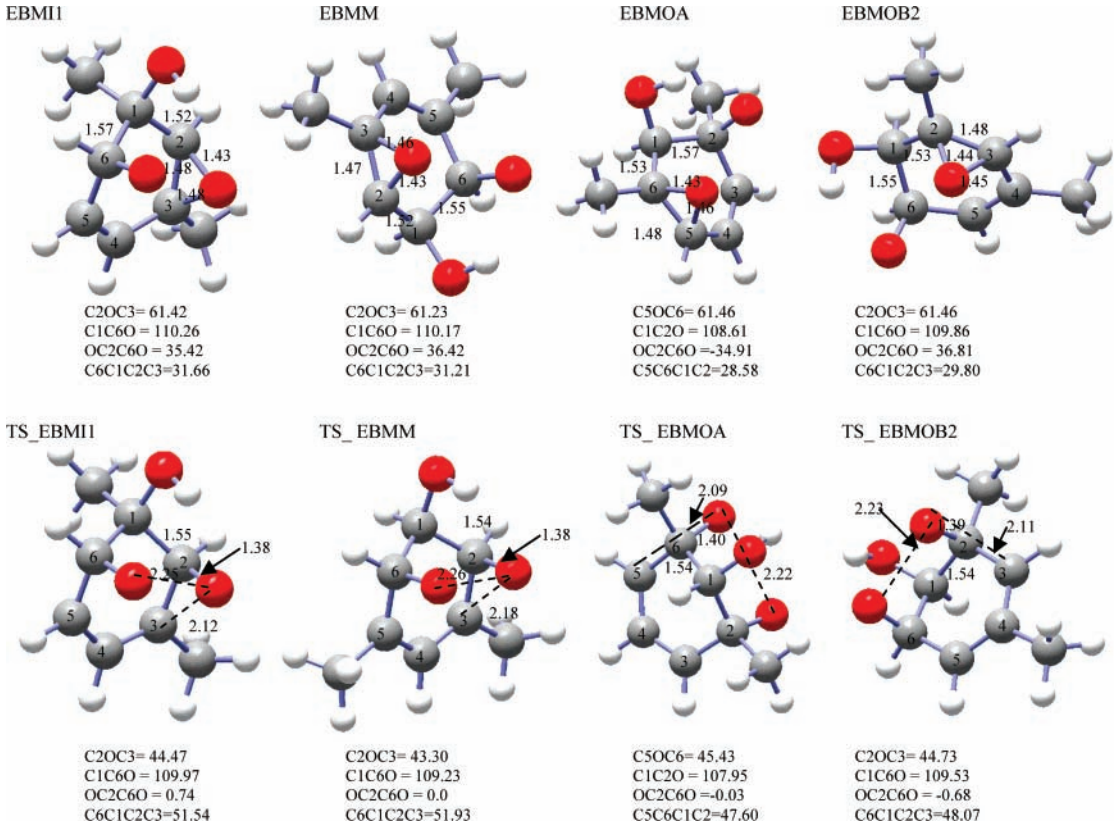

Figure 6. Optimized geometries of the representative epoxy radicals and their corresponding transition states at the B3LYP/6-31G(d,p) level of theory.

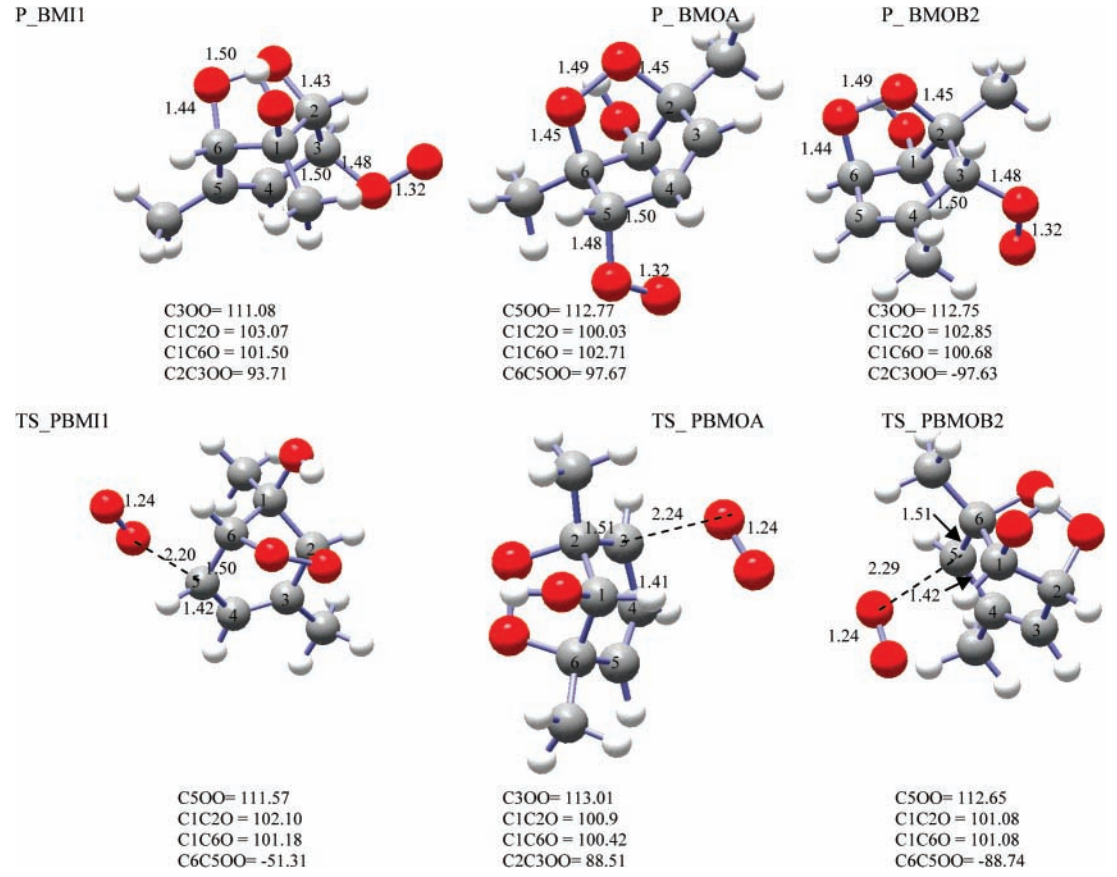

Figure 7. Optimized geometries of the representative bicyclic peroxy radicals and their corresponding transition states at the B3LYP/6-31G(d,p) level of theory.

lower than those for formation of epoxides (Table 3). Therefore, isomerization is the major pathway for the bicyclic radical BMIO. Because the branching ratio for ipso OH addition is very small, the formation of epoxides from this pathway is negligible.

For the bicyclic radicals BMOA and BMOB, which are from the major OH addtion pathways, the effective first-order rates for the O_2 addition to form the bicyclic peroxy radicals are about 10^5-10^6 s^{-1}, comparable to those for isomerization. Because the activation barriers for isomerization are much higher than those for O_2 addition (Figure 5), the formation of epoxides is less possible than the formation of bicyclic peroxy radicals, supporting the most recent experimental study of *m*-xylene reactions with OH for a small yield of the expoxy carbonyls (2−3%).[17] Our present results also agree with the study by Smith et al., indicating that the ring-cleavage pathway involving the bicyclic peroxy radicals represents the major pathway.[4] Considering the steric hindrance associated with another cyclization, the bicyclic peroxy radical likely reacts with NO to form a bicyclic alkoxy radical and NO_2, which is important for ozone formation. The bicyclic alkoxy radicals subsequently undergo ring cleavage, leading to formation of glyoxal, methyl glyoxal, and unsaturated dicarbonyls such as 4-oxo-2-pentenal and 2-methyl-4-oxo-2-butenal, which are the likely components of aerosols from the aromatics.[4−5,17] The large yields of the ring fragmentation products have been observed in several experimental studies.[4,6,17] In contrast to *p*-xylene with a larger probability to form epoxides,[8] the yield of epoxides formed from OH-initiated *m*-xylene oxidation is predicted to be low.

Conclusions

Density functional theory calculations have been performed to elucidate the reaction pathways for the atmospheric oxidation of *m*-xylene initiated by OH radical. OH addition is predicted to occur dominantly at the two ortho positions, with branching ratios of 0.97, 0.02, and 0.01 for ortho, meta, and ipso additions, respectively. The results reveal that the *m*-xylene-OH-O_2 peroxy radicals preferentially cyclize to form bicyclic radicals under atmospheric conditions, rather than reacting with NO to lead to ozone formation. The decomposition of the peroxy radicals to O_2 and the hydroxyl *m*-xylene adducts is competitive with the cyclization process. For the major reaction pathways (two ortho positions), isomerization of the *m*-xylene bicyclic radicals to form epoxy radicals has much higher activation barriers than reaction with O_2, which is in agreement with the experimental studies of a lower epoxide yield and larger yields of the ring-cleavage products of the OH-*m*-xylene reactions.

Acknowledgment. This work was supported by the Robert A. Welch Foundation (Grant A-1417) and Texas Air Research Center (TARC). J.F. was supported by a NASA graduate fellowship. Additional support was provided by the Texas A&M University Supercomputing Facilities. The authors acknowledged the use of the Laboratory for Molecular Simulations at Texas A&M.

References and Notes

(1) Hoekman, S. K. *Environ. Sci. Technol.* **1992**, *26*, 1206.
(2) Olson, K. L.; Sinkevitch, R. M.; Sloane, T. M. *J. Chromatogr. Sci.* **1992**, *30*, 500.
(3) Harley, R. A.; Hannigan, M. P.; Cass, G. R. *Environ. Sci. Technol.* **1992**, *26*, 2395.
(4) Smith, D. F.; Kleindienst, T. E.; Mciver, C. D. *J. Atmos. Chem.* **1999**, *34*, 339−364.
(5) Zhang, R.; Suh, I.; Zhao, J.; Zhang, D.; Fortner, E. C.; Tie, X.; Molina, L. T.; Molina, M. J. *Science* **2004**, *304*, 1487.
(6) Yu, J.; Jeffries, H. E. *Atmos. Environ.* **1997**, *31*, 2281.
(7) Suh, I.; Zhang, R.; Molina, L. T.; Molina, M. J. *J. Am. Chem. Soc.* **2003**, *125*, 12655−12665.
(8) Fan, J.; Zhang, R. *J. Phys. Chem. A* **2006**, *110* (24), 7728−7737.
(9) Suh, I.; Zhang, D.; Zhang, D.; Molina, L. T.; Molina, M. J. *Chem. Phys. Lett.* **2002**, *364*, 454−462.
(10) Suh, I.; Zhao, J.; Zhang, R. *Chem. Phys. Lett.* **2006**, *432*, 313−320.
(11) Kramp, F.; Paulson, S. E. *J. Phys. Chem. A* **1998**, *102*, 2685 - 2690.
(12) Molina, M. J.; Zhang, R.; Broekhuizen, K.; Lei, W.; Navarro, R.; Molina, L. T. *J. Am. Chem. Soc.* **1999**, *121*, 10, 225.
(13) Atkinson, R. *Atmos. Environ.* **1990**, *24*, 1−41.
(14) Perry, (r) A.; Atkinson, R.; Pitts, J. N. *J. Phys. Chem.* **1977**, *81*, 296−304.
(15) Knispel, R.; Koch, R.; Siese, M.; Zetzsch, C. *Ber. Bunsen-Ges. Phys. Chem.* **1990**, *94*, 1375.
(16) Andino, J. M.; Smith, J. N.; Flagan, R. C.; Goddard, W. A.; Seinfeld, J. H. *J. Phys. Chem.* **1996**, *100*, 10967−10980.
(17) Zhao, J.; Zhang, R.; Misawa, K.; Shibuya, K. *J. Photochem. Photobiol. A* **2005**, *176*, 199−207.
(18) Hansen. D. A.; Atkinson, R.; Pitts, J. N. *J. Phys. Chem.* **1975**, *79*, 1763.
(19) Atkinson, R.; Aschmann, S. M. *Int. J. Chem. Kinet.* **1991**, *23*, 77−97.
(20) Nicovich, J. M.; Thompson, R. L.; Ravishankara, A. R. *J. Phys. Chem.* **1981**, *85*, 2913−2916.
(21) Ohta, T.; Ohyama, T. *Bull. Chem. Soc. Jpn.* **1985**, *58*, 3029−3030.
(22) Edney, E. O.; Kleindienst, T. E.; Corse, E. W. *Int. J. Chem. Kinet.* **1986**, *18*, 1355−1371.
(23) Atkinson, R. *J. Phys. Chem. Ref. Data* **1997**, *26*, 215.
(24) Kwok, E. S. C.; Aschmann, S. M.; Atkinson, R.; Arey, J. *J. Chem. Soc., Faraday Trans.* **1997**, *93*, 2847−2854.
(25) Gery, M. W.; Fox, D. L.; Kamens, R. M.; Stockburger, L. *Environ. Sci. Technol.* **1987**, *21*, 339−347.
(26) Tuazon, E. C.; Atkinson, R.; MacLeod, H.; Biermann, H. W.; Winer, A. M.; Carter, W. P. L.; Pitts, J. N. *Environ. Sci. Technol.* **1984**, *18*, 981−984.
(27) Tuazon, E. C.; MacLeod, H.; Atkinson, R.; Carter, W. P. L., *Environ. Sci. Technol.* **1986**, 20, 383−387.
(28) Bandow, H.; Washida, N. *Bull. Chem. Soc. Jpn.* **1985**, *58*, 2541−2548.
(29) Frisch, M. J.; Trucks, G. W.; Schlegel, H. B.; Scuseria, G. E.; Robb, M. A.; Cheeseman, J. R.; Zakrzewski, V. G.; Montgomery, J. A., Jr.; Stratmann, R. E.; Burant, J. C.; Dapprich, S.; Millam, J. M.; Daniels, A. D.; Kudin, K. N.; Strain, M. C.; Farkas, O.; Tomasi, J.; Barone, V.; Cossi, M.; Cammi, R.; Mennucci, B.; Pomelli, C.; Adamo, C.; Clifford, S.; Ochterski, J.; Petersson, G. A.; Ayala, P. Y.; Cui, Q.; Morokuma, K.; Malick, D. K.; Rabuck, A. D.; Raghavachari, K.; Foresman, J. B.; Cioslowski, J.; Ortiz, J. V.; Stefanov, B. B.; Liu, G.; Liashenko, A.; Piskorz, P.; Komaromi, I.; Gomperts, R.; Martin, R. L.; Fox, D. J.; Keith, T.; Al-Laham, M. A.; Peng, C. Y.; Nanayakkara, A.; Gonzalez, C.; Challacombe, M.; Gill, P. M. W.; Johnson, B. G.; Chen, W.; Wong, M. W.; Andres, J. L.; Head-Gordon, M.; Replogle, E. S.; Pople, J. A. *Gaussian 98*, revision D.3; Gaussian, Inc.: Pittsburgh, PA, 1998.
(30) (a) Lay, T. H.; Bozzelli, J. W.; Seinfeld, J. H. *J. Phys. Chem.* **1996**, *100*, 6543−6554. (b) da Silva, G.; Chen, C.-C.; Bozzelli, J. W. *J. Phys. Chem. A* **2007**, *111*, 8663−8676.
(31) Zhang, D.; Zhang, R. *J. Am. Chem. Soc.* **2002**, *124*, 2692.
(32) Lei, W.; Zhang, R. *J. Phys. Chem.* **2001**, *105*, 3808.
(33) Fan, J.; Zhao, J.; Zhang, R. *Chem. Phys. Lett.* **2005**, *411*, 1.
(34) Lii, J. H.; Ma, B. Y.; Allinger, N. L. *J. Comp. Chem.* **1999**, *20*, 1593−1603.
(35) (a) Carpenter, B. K. *J. Am. Chem. Soc.* **1993**, *115*, 9806. (b) Bozzelli, J. W.; Dean, A. M. J. *Phys. Chem.* **1993**, *97*, 4427. (c) Mebel, A. M.; Lin, M. C. J. *Am. Chem. Soc.* **1994**, 116, 9577. (d) Carpenter, B. K. *J. Phys. Chem.* **1995**, *99*, 9801−9810. (e) Barckholtz, C.; Fadden, M. J.; Hadad, C. M. *J. Phys. Chem. A* **1999**, 103, 8108−8117. (f) Fadden, M. J.; Barckholtz, C.; Hadad, C. M. *J. Phys. Chem. A* **2000**, *104*, 3004−3011.
(36) Calvert, J. G.; Atkinson, R.; Becker, K. H.; Kamens, R. M.; Seinfeld, J. H.; Wallington, T. J.; Yarwood, G. *The Mechanisms of Atmospheric Oxidation of Aromatic Hydrocarbons*; Oxford University Press: New York, 2002.